Composites Part C: Open Access 7 (2022) 100236

Contents lists available at ScienceDirect

Composites Part C: Open Access

journal homepage: www.elsevier.com/locate/composites-part-c-open-access

Virtual testing for design and certification of (fusion) bonded longitudinal joints in a fibre composite fuselage: A proposal using FEM-based progressive damage analysis

O. Völkerink *, C. Hühne

German Aerospace Center (DLR), Institute for Composite Structures and Adaptive Systems, Braunschweig, Germany

ARTICLE INFO

Keywords:
Damage mechanics
Finite element analysis (FEA)
Failure criterion
Non-linear behaviour
Plastic deformation
Fibre reinforced plastics

ABSTRACT

In the design of bonded aircraft structures, the type of failure is crucial. More specifically, the failure in case of overload should be limited to the surrounding fibre composite structure. Due to the interaction of damage phenomena, failure behaviour cannot be easily predicted. To simplify the design process, guidelines should ensure that the desired failure behaviour occurs. This work investigates if suitable progressive damage analysis methods can, at least in parts, replace physical test campaigns to substantiate these design guidelines. Using the design of a longitudinal fuselage joint as an example, a continuum damage model for composite materials previously developed by the author is used to analyse the strength and occurring failure modes in detail. It is shown that physical tests could be reduced to a minimum in the future.

1. Introduction

The first applications of today's finite element method (FEM) were in the aerospace industry in the 1950s. The paper from Turner et al. [1] in 1956, in which an aircraft wing structure was analysed, is considered as a starting point of current FEM.

In the past, the use of finite element analysis (FEA) in commercial aircraft design and certification was limited to linear analysis for initial sizing and later for more detailed simulations for certification. Due to conservatism both in methods and material properties this approach demonstrated and ensured an adequate strength of aircraft structures. In the more recent past, advanced nonlinear analysis methods considering plasticity, failure and damage allow for actual strength and failure mode predictions. With the increase in available computing power and further development of methods, there is potential for virtual testing to mitigate risks associated with physical testing or to replace it, at least in part [2].

First applications have already been published: Ostergaard et al. [2] show the virtual test of the Airbus A380 wing and point to the EU FP7 project Maaximus. A major project with Airbus and Dassault Systemes SIMULIA involved making progress towards advanced virtual testing methods. In addition, some recent publications deal with the development of virtual testing methods. Lopes et al. [3] show a roadmap for multiscale virtual testing to efficiently design fibre composite structures. Gigliotti and Pinho [4] have also published a paper on virtual testing of large fibre composite structures. Concepts for a hybrid simulation-physical test pyramid for fibre composites were developed by Tijs et al. [5]. Focusing more on larger structures, Gorskii et al. [6] show virtual test rigs for static strength, fatigue, bird- and hailstrike investigations of aircraft structures. All of this has also led to a certification memorandum from EASA that addresses requirements for modelling and simulation in the context of certification [7].

In parallel, the design of aircraft has moved from metallic to fibre composite structures with thermoset matrix materials [8]. This development continues in the change from thermoset to thermoplastic matrix systems. Aircraft with some components made of thermoplastic-based fibre composites are already in service. Examples are the rudders and elevators from Dassault and Gulfstream business aircraft [9], the leading edge of the Airbus A380 wing and the horizontal tailplane of the AW169 helicopter from Leonardo. Several current research projects focus on technology development for large thermoplastic fibre composite structures [10]. One of the main advantages of thermoplastic-based composites is the possibility of welding or fusion bonding instead of mechanical fasteners or adhesive bonding. This enables changed and more efficient production processes [11] which will be discussed in more detail later.

Although some work on virtual testing has been pointed out, there is still little work that addresses how to incorporate virtual testing methods into the design and certification process. The vast majority of publications focus on the development of the numerical methods

* Corresponding author.
E-mail address: oliver.voelkerink@dlr.de (O. Völkerink).

https://doi.org/10.1016/j.jcomc.2022.100236
Received 10 December 2021; Received in revised form 28 January 2022; Accepted 2 February 2022
Available online 12 February 2022

themselves and on the validation of these with standard test specimens, as can be seen for examples in the reviews [12,13].

For this reason, this study focuses on answering design and certification issues using virtual testing. Illustrated with the example of a fusion bonded longitudinal fuselage joint, this work proposes a design and certification process assisted by virtual testing using progressive damage analyses. First, a brief overview of the certification requirements and design methodologies for composite bonded joints is given. Then the application example with a design issue is introduced. After that, the development of the simulation models for virtual testing with three preliminary studies is described. The work closes with results and conclusions from the virtual test bed as well as a short outlook with a proposed strategy for reduced experimental testing.

2. Virtual design and certification of (fusion) bonded joints

The following section gives a brief overview of the certification requirements, possible design methodologies as well as the challenges during design of bonded structures.

2.1. Civil certification requirements

Starting with a general overview regarding airworthiness certification this subsection deals with the certification of bonded joints in composite structures. Common ways of certification such as certification by tests, by analysis supported by test and by analysis are explained.

2.1.1. Regulations for airworthiness certification

EU Regulation 216/2008 [14] defines common rules in the aviation sector and establishes the European Aviation Safety Agency (EASA). The major objective of these rules is to create and maintain a high and uniform level of safety in civil aviation in Europe. Regulation (EU) No. 748/2012 [15] specifies the application rules for the airworthiness and environmental certification of aircraft and related products, components and equipment, together with the certification of design and manufacturing organisations. This regulation contains an annex, Part-21, which establishes the requirements and procedures for the certification of aircraft and related products, components, equipment and design and manufacturing organisations. In addition to this annex, there are also several certification specifications for different types of aircraft.

The aforementioned airworthiness standards for aircraft (including rotorcraft) cover many aspects like General Design, Structure, Powerplant, Flight, Operating Limits and Instructions. However, none of these sections refer specifically to composites, except one regulation in Certification Specification (CS) 27 for small and CS 29 for large rotorcraft, which relate to fatigue and damage tolerance.

2.1.2. Guidance for certification of composite structures

EASA provides guidance for certification of composite structures in the form of published circulars, policy statements, and memos to clarify the regulations and provide one or more means, but not the exclusive means, of compliance. Applicants have the option to follow the published guidance to streamline the certification process, but may suggest other methods. Although the regulations for metal or composite structures are the same, the means of compliance may vary significantly. The Approved Means of Compliance (AMC) 20–29 "Composite Aircraft Structure" document [16] is a guidance for certification of composite structures published by EASA. It is harmonised with Advisory Circular (AC) 20-107B from the FAA [17] and addresses regulatory requirements with a safety management philosophy [18]. A brief overview of composite structure certification from a regulatory perspective is given by Waite [19].

A major part of the certification is the structural substantiation, which is a process that demonstrates that a design meets the structural requirements [20]. Structural substantiation has to be performed for static strength and damage tolerance considerations. Structural substantiation is a major consideration in certification of civil aircraft. However, many more aspects like durability, crashworthiness, flutter, lightning protection, fire protection and flammability must be considered. These aspects are not discussed in this work. Detailed discussions on certification for civil aircraft can be found for example in [21].

2.2. Design methodology

Since, to the best of the author's knowledge, there is no work on the design of fusion bonded thermoplastic joints in aircraft design, this section reviews and adapts work on adhesively bonded joints.

According to Hart-Smith [22], the main objective of the structural design of adhesively bonded joints is that the bond itself never fails. This means that under all circumstances the adjacent structure fails before a structural failure caused by the adhesive bond can occur. This design philosophy is supported by Waite, who states that "a correctly designed bonded joint is expected to fail in the adherend [...], although failure within the adhesive may occur [...]" [19].

Depending on the design, a bonded joint in a fibre composite structure fails in different ways. In the standard ASTM D5573 a classification of the different failure modes has been published. The standard distinguishes between six different failure modes presented in Fig. 1.

Adhesion or **adhesive failure** describes a disbond at the interface between adherend and adhesive. This failure mode occurs usually due to an inadequate bonding process, especially due to insufficient surface pretreatment. This type of failure must be avoided under all circumstances, as it is considered unacceptable by the authorities [16,17]. For fusion bonded joints in thermoplastic structures, it is rather unlikely.

Cohesive failure refers to a failure purely within the bondline. In this failure mode, the cohesive strength of the adhesive or fusion bond is reached. Thus, the maximum strength of the bonded joint itself is achieved.

Cracks in bonded joints with commonly seen mixed mode ratios of peel and shear stresses tend to propagate towards one adherend [23]. This cohesive failure near the interface of adhesive and adherend is referred to as **thin-layered cohesive failure**.

If failure is located in the adherends near the bond, the failure is termed **fibre-tear** or **light-fibre-tear** failure. The occurrence of these types of failure depend on the transverse properties like interlaminar composite strength and the stacking sequence in the composite adherends.

If the bond strength is greater than the laminate strength, so called **stock-break failure** occurs. In this case, the structure fails due to adherend breakage outside of the bond.

Expressed in failure modes as defined by ASTM D5573, stock-break failure is the desired mode. Based on Hart-Smith's statement, Davis and Bond have proposed a certification methodology for bonded joints [24]. The proposed methodology is based on a comparison between the load capacity of the bonded joint (in shear) with the different design load cases. Davis and Bond distinguish between five possible conditions which are described in the following:

- **Condition 1:** The load capacity of the bond is greater than the ultimate strength of the composite material which forms the joint. Thus, failure by shear through the bondline should never occur.
- **Condition 2:** The load capacity of the bond is greater than the known Structural Ultimate Load (SUL) of the surrounding structure, but less than the ultimate strength of the composite material which forms the joint. Therefore, there should never be a failure due to shear caused by the bondline itself, because the structure away from the joint will fail beforehand.

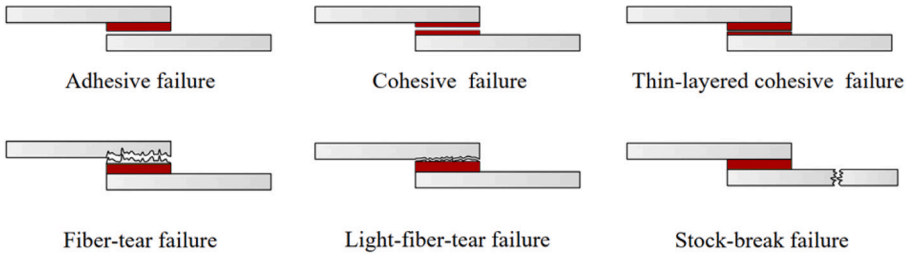

Fig. 1. Sketches illustrating failure modes according to ASTM D5573.

- **Condition 3:** The load capacity of the bond is less than the known SUL, but greater than the design Design Ultimate Load (DUL) of the surrounding structure. Because the structural loads should never exceed DUL, failure by shear through the bondline should not occur. Nevertheless, the bondline is the weakest element of the joint and when the structure is tested to SUL, failure occurs in the bond.
- **Condition 4:** The load capacity of the bond is greater than the design Design Limit Load (DLL) for the surrounding structure, but less than the DUL. Joints showing this strength condition are only suitable for reinforcement repairs where the structure to be repaired can sustain certification requirements also without the repair.
- **Condition 5:** The load capacity of the bond is less than DLL for the surrounding structure. Joints showing this strength condition are only applicable where aircrafts are operated under flight restrictions, because if operating loads were not restricted, failure by shear though the bondline is possible.

This methodology is adopted for the fusion bonded longitudinal fuselage in this work. Based on these considerations, during the design process the design engineers must check in which failure mode their current bonded joint design is likely to fail. The failure mode is affected by many design parameters like joint geometry, layup and material of the composite adherends, as well the mechanical properties of the (fusion) bond itself. An overview of failure mode driving design parameters is given in [25,26].

Because of the many failure mode influencing design parameters, it is a complex task to predict the strength and failure mode of a joint design. If cost- and time expensive structural testing of each design version shall be avoided, the design engineer needs capable analysis methods to predict the mechanical behaviour up to total failure during the design process.

3. Application example: longitudinal fuselage joints

This section introduces the application example for the proposed virtual testing-based methodology for design and certification in detail. Starting with the Multifunctional Fuselage Demonstrator (MFFD), which serves as reference structure, loads on the longitudinal joint are briefly introduced as well as the design variants to be investigated. This section concludes with the problem statement, which is considered in detail in this work: The positioning accuracy of the two fuselage half-shells and its effect on the mechanical performance of the joints.

3.1. Longitudinal joint of multifunctional fuselage demonstrator

The aviation sector is estimated to be responsible for 2%–3% of global CO_2 emissions with an expected doubling of emissions by 2050 [27]. As flying brings economic benefits and connectivity, ways must be found to reduce emissions. Mass reduction is one of the approaches since 100 kg mass reduction is estimated to save 600000 litres of fuel in an aircraft life [28].

This is already done by the aircraft manufacturers by replacing metallic alloys with fibre composite materials. Most advanced fibre composite aircraft structures are made from continuous carbon or glass fibres with a thermoset polymer matrix material. These materials are well developed, have competing prices, mature manufacturing processes and well-established supply chains. Though, they are manufactured in a long and labour intense manufacturing process and have only limited recycling possibilities. Due to this, high-performance thermoplastic matrix materials are considered as an alternative. Thermoplastics can be processed by heating above their glass transition temperature and do not crosslink or cure like thermoset materials. [29]

However, one of the main advantages of thermoplastics is that they can be heated and cooled down multiple times without loss of mechanical properties and therefore they can be welded or fusion bonded [30,31].

As mentioned in the introduction, there are already some certified and flying components made of thermoplastic composites [9]. But a complete aircraft fuselage made of this class of material does not yet exist. For reason, the MFFD made from thermoplastic composite material was conceived for research and technology development [11]. The possibility of fusion bonding, a dustless joining process, is important for the concept. Unlike before, where holes have to be drilled and mechanical fasteners installed to join the parts, with fusion bonding electrical systems can be installed prior to assembling the aircraft structures because no conductive carbon fibre chips are produced [11]. This allows for large pre-equipped sub-assemblies with a high cost saving potential.

This enables the concept of a lower and upper fuselage half shell with a high level pre-installation of system prior to final assembly line. The multifunctional fuselage demonstrator features the asymmetrical single-aisle fuselage of the Airbus A321. It is built from four main modules: The upper and lower shells as well as a floor and a crown module with the main systems. The dimensions of the demonstrator are 8 m in length and a varying radius between 2 m and 2.5 m [29]. The fusion bonded longitudinal joint between the lower and upper shell of the fuselage is the object of investigation in this work. In the description of the demonstrator, LM-PAEK is provided as material. However, due to the availability of material characteristics, the study in this work is carried out with the very similar material AS4/PEEK. A CAD visualisation of the demonstrator can be seen in Fig. 2. More details of the MFFD and the manufacturing concept are published in [11,29].

3.2. Loads on the longitudinal joint

The main loads on aircraft fuselages are manoeuvring and gust, internal cabin pressure, landing procedure and ground handling [32]. However, the primary loading for the fuselage skin and therefore for the longitudinal joint is hoop stress caused by the difference between atmospheric and the cabin pressure [33]. These hoop stresses, resulting in a tensile loading of the longitudinal joint in circumferential direction, are used for the joint design.

The decisive factor for sizing is the maximum pressure difference between internal and external pressure. Typically, the aircraft internal

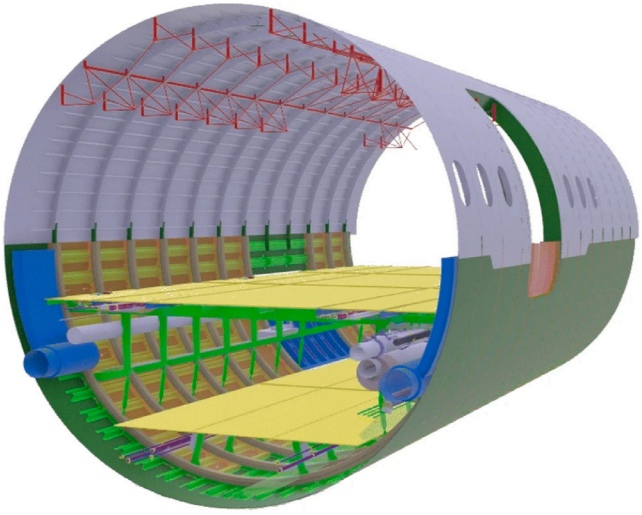

Fig. 2. An overview of the multifunctional fuselage demonstrator from [29].

pressure is 0.075 MPa which corresponds to an altitude of 8000 ft. The average maximum altitude of commercial aircraft is 45000 ft, which corresponds to an air pressure of 0.015 MPa. This results in a pressure difference of 0.06 MPa [33]. According to CS 25, this maximum expected load is referred to as the DLL. If not further specified, a safety factor sf of 1.5 has to be considered for the structure, this results in the DUL. For pressurised components of aircraft operating up to an altitude of 45000 ft an additional sf of 1.33 shall be applied:

$$DUL = DLL \cdot sf = DLL \cdot 1.5 \cdot 1.3 = 2.0 \cdot DLL \tag{1}$$

The hoop stress σ_h can be calculated from the pressure p, the radius of the fuselage R and the skin thickness t with:

$$\sigma_h = p \cdot \frac{R}{t} \tag{2}$$

With a skin thickness of 2.208 mm the equation above results in a hoop stress of $\sigma_z = 86.14$ MPa. Niu [32] states that, depending on aircraft type, the hoop stress varies between 80 and 110 MPa.

A more advanced analytical solution for the hoop stress considering circumferential and axial stiffening elements is given by Flügge [34]. However, the simple approximation is sufficient for this consideration.

3.3. Design variants to be investigated

Three different design variants are investigated in this study. The configuration A1, cf. Fig. 3, is a simple single overlap joint. The thermoplastic fibre composite fuselage skin consists of two sublaminates, each of which has the layup [45°,-45°,0°,90°,-45°,45°]. The initial overlap length of the fusion bond is 60 mm.

The second variant under investigation is configuration A2. Again, the fuselage skin is made from two sublaminates, but in A2 the joint is formed as an stepped lap joint with two steps. Each step has a length of 30 mm. In this way the same initial bonding area as for configuration A1 is achieved.

Like configuration A2, the third variant A3 is a stepped joint. The difference is a thicker fuselage skin. In the A3 variant, the skin consists of three sublaminates and the joint is formed by three steps with 30 mm length each.

The configurations A2 and A3 are illustrated in Figs. 4 and 5. Common to all configurations is that by using the sublaminates, the fusion bonded interface has a 45° fibre orientation.

3.4. Positioning accuracy of the fuselage halves

As described in the section on the MFFD, the pre-equipped fuselage half-shells shall be joined by thermoplastic welding with a target overlap length of a few centimetres. One of the major challenges during joining is the positioning of the components, which are quite large with 8 m in length and 4 m in diameter and, due to the pre-equipment, also heavy and sensitive. The positioning accuracy in circumferential direction that can be tolerated in the design is therefore a decisive parameter for the complexity of the joining process. A larger tolerance range for the overlap length simplifies and speeds up the joining process, thus saving costs. As an example, Fig. 6 shows the configuration A2 with the defined step length of 30 mm but with an overlap of only 15 mm and a gap of 15 mm.

The progressive damage analyses based design process proposed in this work is used to determine the strength and failure mode of the different configurations with varying gap length. In this way, the largest allowable tolerance will be determined without physical testing.

4. Simulation model for virtual testing

This section briefly describes the requirements for the simulation models, simplifications, loads and boundary conditions, the material modelling as well as element size considerations. Preliminary simulations have shown that the strong non-linearities due to plasticity and damage leads to some models not converging with Abaqus/Standard. For this reason, all simulations in this study are performed using Abaqus/Explicit Version 2020. More details on the simulation hardware and runtimes are given in Section 5.

4.1. Requirements

To be able to predict the strength and failure behaviour of the different design variants with different gap lengths, the relevant failure mechanisms must be captured by the simulation method used. This includes the behaviour of the thermoplastic fibre composite adherends up to total failure as well as damage of the fusion bond itself. The material model used for the composite adherends should include failure criteria as well as damage progression models for fibre and matrix failure. The latter should be captured in-plane as well as out-of-plane (delamination failure). Whether modelling the plasticity of the composite adherends is necessary or not is investigated in this study.

In addition, to use simulations for certification purposes in the future, the requirements stated in the EASA certification memorandum regarding modelling and simulation in the context of certification of CS-25 aircraft [7] have to be fulfilled. The requirements are not fully met in this study as this work is intended to be a proposal for a way in which simulations can be used in the context of future design and certification activities.

4.2. Modelling simplifications

The design of aircraft longitudinal fuselage joints is mostly based on the results of static and dynamic tests of uniaxially loaded flat specimens [33]. With regard to the actual conditions, not only the real (much larger) dimensions and the surrounding connections to other structural components are neglected, but also the influence of the curved fuselage structure. That these simplifications are justified is shown by their application in practice over many years with sufficiently good results to consider them within a design. However, uncertainties are absorbed by large safety factors [35].

At this point, at least the effect of curvature should be briefly explained in some detail. So far, only a few investigations on overlap joints of curved structures can be found in the literature. One example is given by Parida and Pradhan [36]. Among other things, the influence of a variable radius of curvature on the strength of a composite lap joint

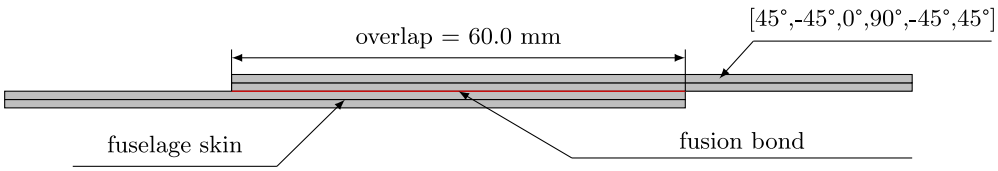

Fig. 3. Configuration A1.

Fig. 4. Configuration A2.

Fig. 5. Configuration A3.

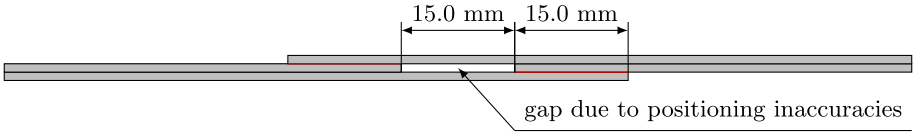

Fig. 6. Configuration A2 with 15 mm gap.

is investigated. The energy release rate is used as an indicator of crack growth and delamination processes. The findings of Parida and Pradhan are that failure processes are always multiaxial and that flat lap joints (infinite radius of curvature) generally have a higher resistance to crack growth than curved ones. Comparable statements are also made by Liu et al. [35]. In their study, the joint strength of curved structures is analysed using cohesive zone modelling. Liu et al. state that the effect of moderate curvatures on the maximum bearable load of a joint is negligible. More specific, they show that, as the radius of curvature decreases, the peel stresses at the overlap ends change from tensile to compressive. Liu et al. recommend to neglect curvature in the joint design if the radius of curvature is greater than 2000 mm, otherwise the curvature should be considered. This recommendation results from a variation of radii of curvature with a step size of 1000 mm. The radius of the MFFD considered in this work is 1950.5 mm on average. As this is close to the described limit, the recommendation of a flat modelling approach is used.

As described before, in this study only tensile loads on the joint due to cabin pressure are considered. By neglecting the loads in the longitudinal direction of the fuselage, the problem can be modelled in 2D by using the plane strain assumption [37]. This state can be used if displacements in a three-dimensional component occur only in two spatial directions or if forces acting in one plane do not cause displacements perpendicular to this plane. This is the case, for example, with planar components, if the expansion in the depth direction is considerably greater than in the other directions. Thus, the modelling of a cross-section (2D) is sufficient and displacements in depth direction may be neglected. However, the single plies of the composite adherends shall be modelled for the progressive damage analysis. This is, at least for the ± 45°-plies, not possible in Abaqus using plane strain elements because the fibre orientation would have to be rotated out of the shell plane and, therefore, a full 3D model is necessary. In order to save computational effort a model with small expansion in the longitudinal direction of the fuselage is used in this study. Using advanced coupling constraints, which will be explained in detail in the next section, by complete elimination of finite width effects a plane strain state is generated in the model. In this way, size and calculation times of the models can be significantly reduced.

4.3. Loads and boundary conditions

This subsection describes the loads and boundary conditions of the simulation models which are used to eliminate finite width effects. They are illustrated using the example of configuration A1, cf. Fig. 7. First, the conditions at the two edges in circumferential $x-$direction are described. The left side of the model ($x = 0$) is fully constrained ($u_x = u_y = u_z = u_{rx} = u_{ry} = u_{rz} = 0$), whereas, on the opposite side ($x = l$) a load is applied as a displacement. In addition, at this edge ($x = l$) the displacements in the $y-$ and $z-$directions are suppressed ($u_y = u_z = 0$).

Like described in Section 4.2, a stress state like in the middle of an infinitely wide structure must be achieved in the simulation model. This requires special boundary conditions which rely on coupling of displacements. A simple coupling only of the free edges of the model ($z = 0$ and $z = b$) is only sufficient if parts with isotropic materials or composites with longitudinal and/or transverse fibre orientations are coupled. However, if the parts also contain layers with off axis fibre orientations, like ±45°, simple coupling results in edge effects [38]. This is the case in the present application example. Therefore, more advanced coupling conditions have to be used. This is done by adopting the coupling conditions described by Al-Ramanhi et al. [38]. In the following, a brief overview of the advanced coupling conditions is given.

The first coupling involves nodes on the free edges of the model ($z = 0$ and $z = b$). The $z-$displacements of nodes that have the same $x-$coordinate and are consequently on a vertical line are coupled. This is illustrated in Fig. 8. The coupling is applied along the length of the model on every set of nodes sharing the same $x-$coordinate, but on both edges ($z = 0$ and $z = b$) separately. In this way, all nodes on these vertical lines have the same displacement u_z:

$$u^m_{z-coupled} = (x_m, Y, 0); u^m_{z-coupled} = (x_m, Y, b) \tag{3}$$

The index m describes the variable $x-$position, Y includes all nodes of a vertical line and 0 or b indicates the position of the edge ($z-$position).

The second coupling runs through the width of model and couples the $x-$ and $y-$displacements of nodes, which lie on a line in depth direction, compare Fig. 9. Every node in the model is affected by this coupling. In contrast to the first condition, the lines of the coupled

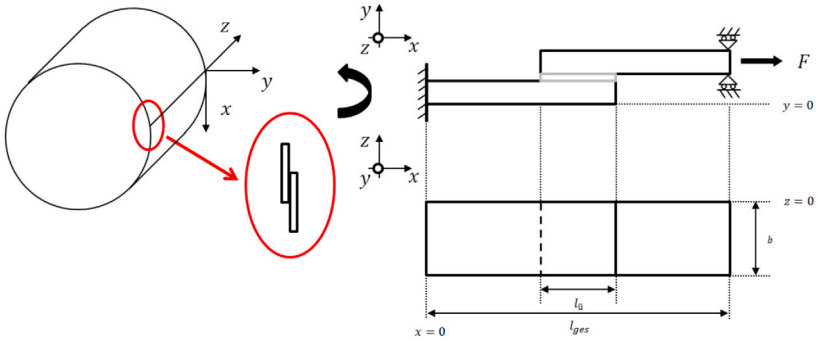

Fig. 7. Coordinate system used for the aircraft fuselage as well as geometry, boundary conditions and coordinate system of the simulation model.

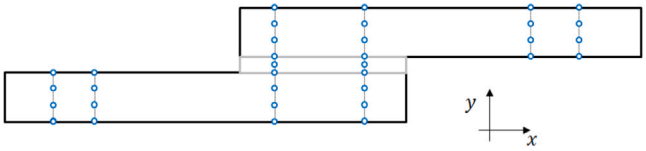

Fig. 8. Front view for coupling of displacement u_z applied on the nodes with the same x−coordinate belonging to the vertical lines on the edge.
Source: Adopted from [38].

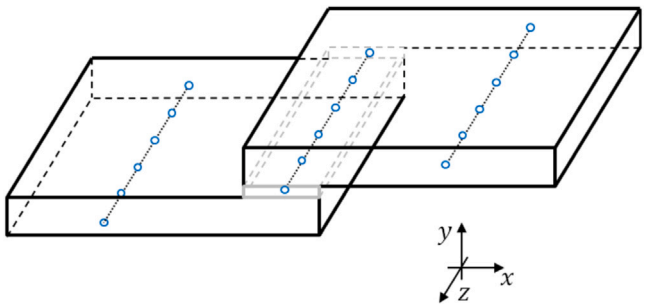

Fig. 9. Coupling of u_x and u_y on nodes belonging to lines through the width of the joint.
Source: Adopted from [38].

nodes are not only on one variable coordinate, but on two. Ergo, a second position index n has to be introduced:

$$u^{m,n}_{z-coupled} = (x_m, y_n, Z); u^{m,n}_{y-coupled} = (x_m, Y_n, Z) \quad (4)$$

By introducing this coupling conditions, edge effects are not completely eliminated, but strongly reduced. This allows reducing the width of the model to a minimum without noticeably changing the result. A width study to prove this and find a width for the virtual testing of the different joint configurations is presented in Section 5.

4.4. Modelling of thermoplastic composite adherends

A user-defined material model developed by the authors [39] based on Continuum Damage Mechanics (CDM) is used to describe the mechanical behaviour of the AS4/PEEK adherend material.

The material model features the transversely isotropic plasticity model by Sun and Chen [40], which can be deactivated for computational efficiency. If the model is deactivated, the adherends are modelled linear-elastic up to the damage initiation. This saves calculation time at the expense of accuracy.

Failure initiation is detected using the Failure Mode Concept by Cuntze [41] which distinguishes five different failure modes. These are FF1 and FF2 for fibre failure in tension and compression as well as IFF1 to IFF3 for interfibre failure in tension, compression and shear. The progressive damage after failure initiation is modelled by using an energy-based strain-driven linear degradation model.

Since the material model is fully 3D and used in combination with reduced integrated solid elements (C3D8R), discrete modelling of delaminations between the plies of the adherends is not required and therefore omitted.

The material and model parameters used in this work can be found in Table 1. The elastic as well as the plastic properties are adopted from Sun and Yoon [42]. The values for tensile and shear strengths are taken from Kawai [43] whereas the compressive strengths are obtained from Sun and Rui [44]. The values for the critical strain energies are adopted from Carlile et al. [45] and Chen et al. [46].

Since the required parameters for Cuntze's FMC were not available for AS4/PEEK, the values determined by Petersen et al. [41] for M21/T700GC, a material with a tough epoxy matrix, are used. The parameters are listed in Table 2.

The in-plane edge length of the elements is determined to 0.83 mm using the approach by Bažant and Oh [47] to avoid local snap backs during degradation. A more detailed description of the model including a validation with open hole tension specimens also made from AS4/PEEK and a mesh study can be found in [39].

Table 1
Intralaminar material properties and model parameters for AS4/PEEK.

E_{11}	$E_{22} = E_{33}$	$G_{12} = G_{13}$	G_{23}	$\nu_{12} = \nu_{13}$	ν_{23}
126.7 GPa	10.3 GPa	6.0 GPa	3.45 GPa	0.32	0.49
$R^t_{\parallel}$	$R^c_{\parallel}$	$R^t_{\perp}$	$R^c_{\perp}$	$R_{\perp\parallel}$	η
2023.0 MPa	1234.0 MPa	92.7 MPa	176.0 MPa	82.6 MPa	0.0002
$G_{ft} = G_{fc}$	$G_{mt} = G_{mc}$	G_s	a	α	β
128.0 kJ/m^2	5.6 kJ/m^2	4.93 kJ/m^2	1.5	0.142857	295.0274

Table 2
Parameters for FMC by Cuntze.

$b_{\perp\parallel}$	$b_{\perp\perp}$	m
0.44	1.266	2.6

4.5. Modelling of fusion bonded joint

In this work, cohesive zone modelling [48] is used to describe the debonding of the fusion bond between the adherends. More specifically, cohesive surfaces are used. The initiation of damage is predicted with a stress-based quadratic power law as proposed by Ye [49] as this criterion was successfully applied in previous studies [48,50,51]. For mixed-mode damage propagation the criterion by Benzeggagh and Kenane is utilised [52]. The material and model parameters used in this study summarised in Table 3 are taken from [50].

Table 3
Interlaminar material properties and model parameters for AS4/PEEK from [50].

G_{Ic}	G_{IIc}	η_{BK}	T_I	$T_{II} = T_{III}$	$K_I = K_{II} = K_{III}$
0.969 kJ/m^2	1.719 kJ/m^2	2.284	80 MPa	100 MPa	10^6 N/mm^3

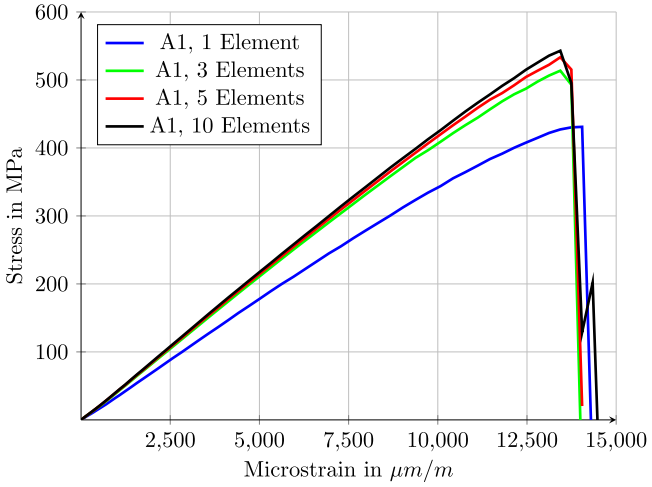

Fig. 10. Stress–strain curves from configuration A1 with model widths.

5. Preliminary studies for modelling

In this section, three preliminary studies are conducted to determine the final modelling for the main study to find the maximum tolerable gap of the fusion bonds. Firstly, the width of the simplified model is investigated and secondly, the need to consider plasticity is studied. In addition, a brief section on validation can be found at the end.

5.1. Investigation of the required model width

Configuration A1 with the nominal overlap length of 30 mm is taken as an example for the width study. For this purpose, four models were set up and simulated, differing only in width. The width varies from one element to three and five, up to a maximum of ten elements. For this variation the element size is kept the same, so that the absolute width of the model varies from 0.83 mm to 8.3 mm. The results in the form of a stress–strain diagram are shown in Fig. 10. The model with one element width results in the lowest stiffness, which is significantly lower than the stiffness of the remaining models. This is attributed to the fact that the coupling conditions at the two free sides of the model are applied on the same element. The predicted strength is also the lowest of the models. The difference in stiffness and strength between the models decreases with increasing model width. The strength predicted with the three-element model is 5.3% lower at 514 MPa than the strength of the ten-element model at 543 MPa. The five-element model gives a strength of 533 MPa, which is only 1.8% lower than the widest model.

In Table 4 the wallclock time of the simulations using one CPU core on a workstation with an Intel® Xeon® E5-2670 v3 processor and 48 GB RAM is given. Considering the simulation runtimes, the model with five elements is chosen as a compromise between runtime and accuracy. It is not substantially less accurate, but requires with 43670 s to 141555 s wallclock time less than half of the runtime of the 10 elements model.

5.2. Influence of plasticity of composite adherends

As described earlier in this work the consideration of plasticity is optional in the material model for the fibre composite. To study the influence of plasticity, at first a coupon tension tests from [53] with

Table 4
Wallclock time for the different model widths.

Model width	Wallclock time in s
1 Element	6460
3 Elements	24755
5 Elements	43670
10 Elements	141555

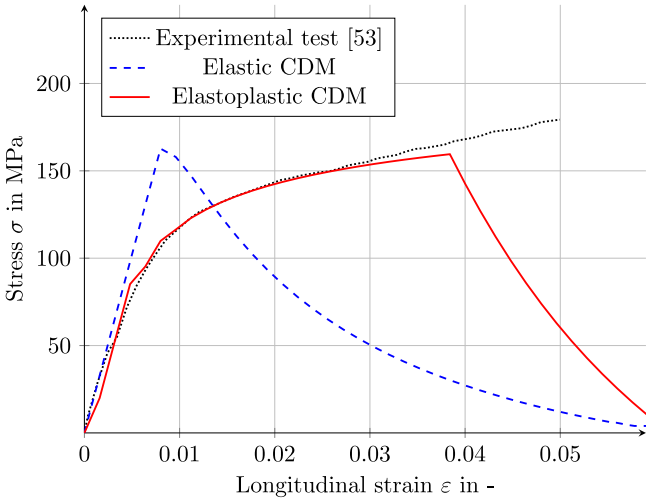

Fig. 11. Experimentally and numerically determined stress–strain curves of an AS4/PEEK $[\pm 45°]_{2s}$ tensile test.

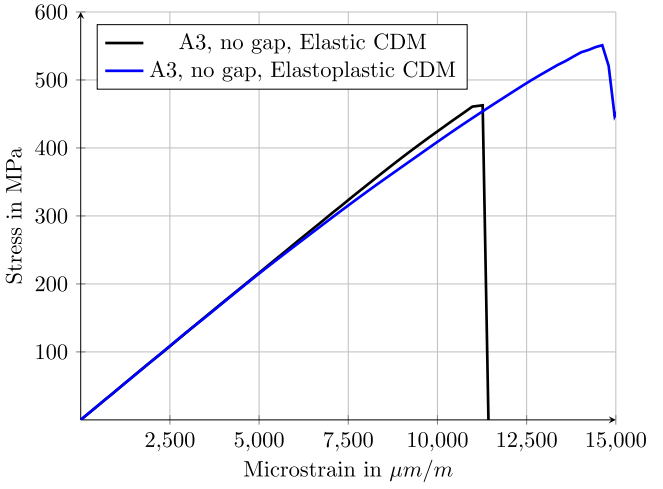

Fig. 12. Influence of plasticity of composite adherends — stress–strain curves from configuration A3 without gap.

±45°-fibre orientation is simulated with and without plasticity. The results are shown in Fig. 11.

It is obvious that the model with plasticity represents the test much better. In particular, the failure strain is strongly underestimated by the model without plasticity. However, since this is an extreme example due to the ply layup, a second comparable simulation is carried out on Configuration A3 with the nominal overlap length of 30 mm. The results are shown in Fig. 12.

In contrast to the coupon example, not only the failure strain is higher for the model with plasticity, but also the determined strength (463 MPa to 551 MPa). This is attributed by the author to the possible load redistribution in the joint after yielding. Since the material behaviour, as previously shown, can be modelled more realistically

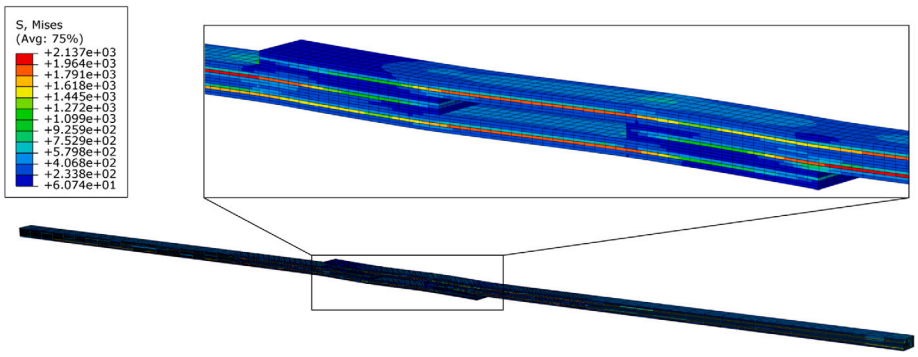

Fig. 13. Stress field (von Mises) in configuration A2 with 15 mm gap at a loading of 524 MPa.

with plasticity and the results for the object of investigation A3 differ significantly, all subsequent simulations are carried out with plasticity.

5.3. Validation of modelling approach and material data with single lap shear joints

No own experimental tests were carried out in the context of this study, as it is intended to show a way to use progressive damage analyses in design of fusion bonded joints. However, it should be ensured that the material modelling is appropriate and the used material parameters are realistic. The validation of the intralaminar modelling approach using the user-defined material model with open hole tension specimens can be found in a previous study of the authors [39]. It is performed like in this study performed with AS4/PEEK material.

Nevertheless, the modelling of the fusion bond with cohesive surfaces as well as the simplified model without width effects are not validated. This is carried out in brief using single lap shear strength values from literature. This is not a thorough validation, but is intended to show that the model can in principle deliver realistic results.

In the review paper from Ageorges et al. [30] on fusion bonding of thermoplastic composites, an overview of lap shear strength values depending on the fusion bonding technique is given for AS4/PEEK. Smiley et al. [54] report a lap shear strength of 40 MPa when the fusion bond is achieved by bulk heating. For the common technique of ultrasonic welding the majority of the authors measured lap shear strengths between 34 MPa [55] to 35 MPa [56] and 40 MPa [57].

With the single lap shear joint configuration of Smiley et al. [54], a simulation was performed using the modelling technique described above with the five element wide model. Smiley et al. used a $[0,45,90,-45]_{2s}$ layup in a 25 mm wide joint with 12.5 mm overlap length.

The simulation gives a lap shear strength of 34.8 MPa. This value lies in the lower range of the literature data. Thus, the modelling approach in this study basically outputs realistic, albeit slightly conservative, strengths.

6. Results from virtual test bed and discussion

This section covers the results from the virtual test bed with focus on strength and failure behaviour of the different design variants. A design guideline for positioning accuracy is derived and an outlook regarding a proposed strategy for reduced experimental testing is given.

6.1. Stress field at the example of configuration A2

At the example of configuration A2 with a 15 mm gap the stress field occurring in the model is investigated. The stress field in terms of von Mises stress is shown in Fig. 13 at a loading of 524 MPa which is prior but close to total failure. As expected, especially the 0° plies are highly loaded up to a value of 2137 MPa. The highly loaded areas are located at the outer overlap edges as well as in the vicinity of the gap where the cross section is reduced.

In addition, at the same load level of 524 MPa the damage in the fusion bond is shown in Fig. 14. It is expected that the coupling constraints introduced in Section 4.3 lead to a constant damage across the width. This would show that the five element wide strip of the fuselage skin with the fusion bond behaves like in a infinite wide panel and a plane strain state is achieved. From Fig. 14 it can be seen, that this is in general attained. Except from the two diagonal corners of the inner edges facing the gap, the damage values are constant across the width. This is considered sufficient by the authors, as the deviation only affects one integration point in each case.

6.2. Strength and failure behaviour of the design variants

In Fig. 15, 16 and 17 the stress–strain curves from the simulations of the configurations A1, A2 and A3 are shown. All configuration are simulated with the initial overlap length. These results are marked as no gap. In addition, models with gap length of 10 mm, 15 mm and 20 mm are simulated for all three variants. This results in remaining fusion bond lengths of 20 mm, 15 mm and 10 mm per step. In general, the stiffness of the variants A1, A2 and A3 as well as strength and failure strain are very similar. The non-linearity at high loading increases from configuration A1 to A3. The strength level of configuration A1 is slightly lower than the strength of A2 and A3. The strength of A1 without gap is slightly lower at 533 MPa, compared to 558 MPa for configuration A2 and 551 MPa for configuration A3. This is attributed to the reduced secondary bending of the stepped joints. Furthermore, an extension of the gap length from no gap at all up to 15 mm has only minor impact on strength and failure strain of all configurations. A gap length of 20 mm, on the other hand, which is shown in the diagrams with dashed curves, leads to a considerable reduction in strength for all configurations. At 372 MPa, configuration A1 shows the largest strength drop, but the strength of A2 (501 MPa) and A3 (499 MPa) is also significantly reduced. All variants withstand significantly more than the DUL of 90–120 MPa described in the section on loads for all considered gap lengths. Nevertheless, besides the pure load capacity, as stated before, there is also a requirement for the failure mode. Therefore, the failure mode is considered in more detail.

Configuration A2 is taken as an example to compare the failure modes between the models with 15 mm and 20 mm gap length. Thus, between the models where there is a significant drop in load. Though, up to 15 mm gap length the joints fail near the fusion bond, the final failure is caused by breakage in the composite adherend modelled with the user-defined continuum damage model. This can be seen in Fig. 18(a).

With 20 mm gap length the composite adherends remain nearly intact, but the fusion bond itself, modelled with the cohesive surfaces, fails, cf. Fig. 18(b). This change in failure mode between 15 and 20 mm gap length can be observed in all configurations. The observed failure modes are also indicated in the legend of the stress–strain plots in Fig. 15 to 17.

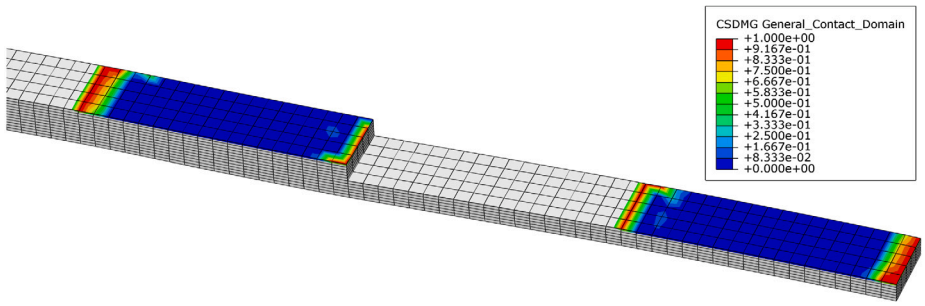

Fig. 14. Damage in fusion bond of configuration A2 with 15 mm gap at a loading of 524 MPa.

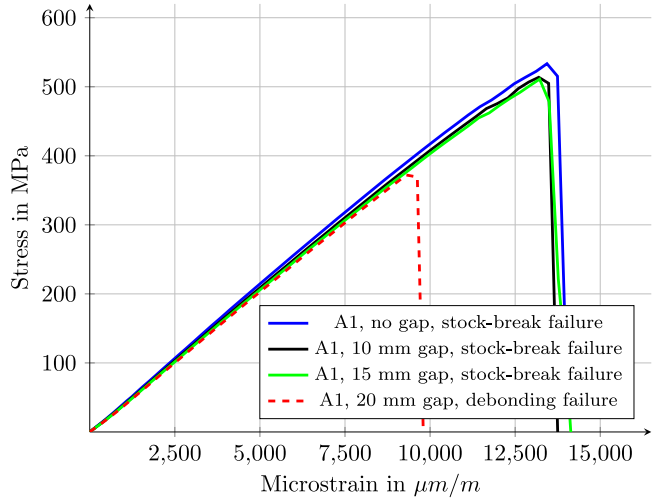

Fig. 15. Stress–strain curves from configuration A1 with different gap lengths.

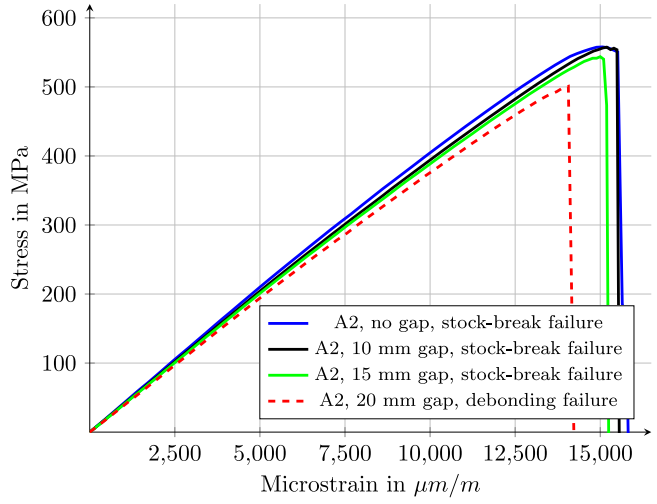

Fig. 16. Stress–strain curves from configuration A2 with different gap lengths.

6.3. Design guideline for positioning accuracy

A design guideline with regard to positioning accuracy can now be derived from the virtual test bed results. First, all three investigated configurations meet the requirements. It is confirmed that the strength is sufficient even with an inaccurate positioning of 20 mm. However, then, with the remaining joint length of only 10 of the initial 30 mm, the failure mode for all configuration change from stock-break to cohesive or debonding failure. With regard to the previously introduced design methodology from Davis and Bond [24] as well as Hart-Smith [22] this is not tolerable. It must therefore be ensured during manufacturing that an overlap length of at least 15 mm is fusion bonded from the initial overlap of 30 mm to ensure the desired failure mode.

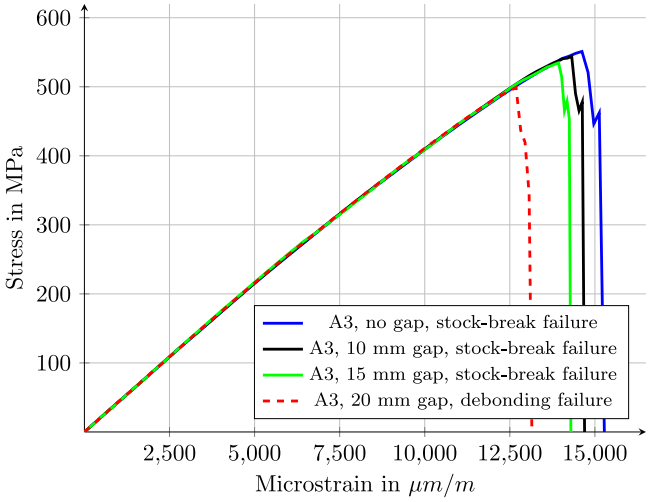

Fig. 17. Stress–strain curves from configuration A3 with different gap lengths.

6.4. Outlook: proposed strategy for reduced experimental testing

Using the example of the longitudinal fuselage joint, a strategy for reducing physical testing can be derived. To allow for the largest possible tolerance in the overlap at which the joint still fails in the desired failure mode, an extensive experimental test campaign with varying gap lengths has been necessary so far. With the capability of newly developed progressive damage analysis methods, the gap length where the failure mode changes can be found by virtual testing. It is then only necessary to experimentally validate the region in which the change of failure mode occurs. This is illustrated in Fig. 19. This significantly reduces the amount of expensive physical testing. Of course, this requires numerical methods that are further validated than the method in this paper. Furthermore, as required by EASA [7], in addition to the uncertainty quantification (UQ) for experimental tests, UQ is also required for virtual tests.

7. Conclusion: decisive change in failure mode

This work shows the potential of virtual testing in the design and certification of (fusion) bonded joints using FEM-based progressive damage analysis. The design of a fusion bonded longitudinal joint in an aircraft fuselage made from thermoplastics-based fibre composite material serves as an example to showcase the proposed method.

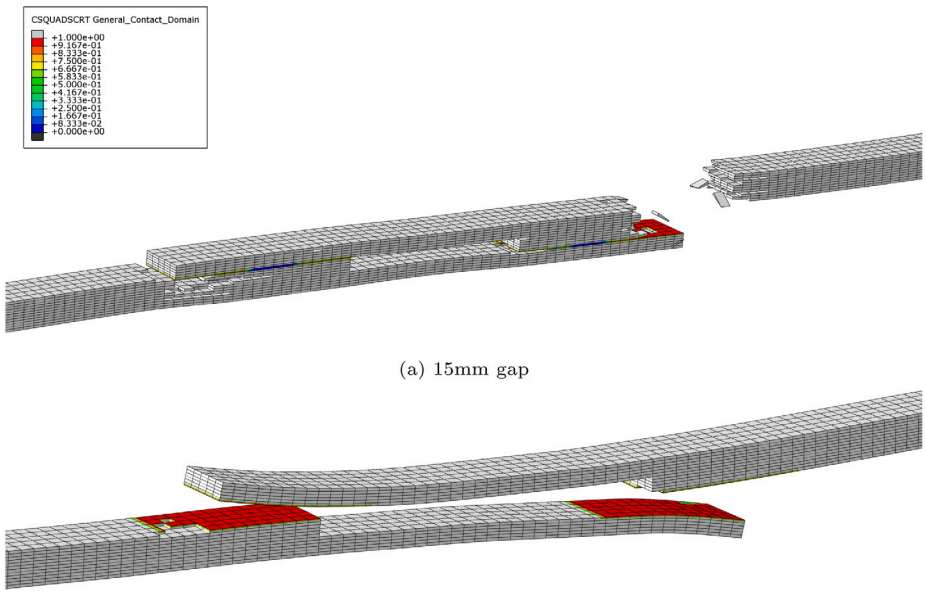

(a) 15mm gap

(b) 20mm gap

Fig. 18. Configuration A2: change in failure mode from 15 mm gap (stock-break failure) to 20 mm gap (debonding failure).

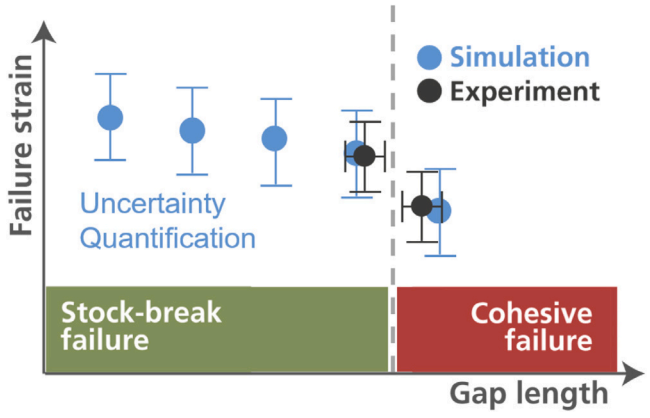

Fig. 19. Illustration of the proposed strategy to reduce physical testing.

Taking advantage of the plane strain condition and limiting the main load case to the one resulting from cabin pressure, virtual structural tests can be realised with manageable computation times. This allows not only to determine the behaviour of different design variants, but also to numerically investigate further parameters, such as the influence of the overlap length on the failure behaviour. Designers thus gain not only a tool to validate designs, but also get a deeper understanding of the effective mechanisms in the joint.

To join two half-shells of the example into a fuselage section, two large components must be aligned very precisely. The required positioning accuracy and the resulting overlap length of the fusion bond influence the assembly effort and consequently the production costs significantly. Based on the nominal overlap length, the proposed method is used to find the minimum possible length at which the failure mode does not change. By doing so, it is ensured that the failure in case of an overload does not occur in the bond itself, but remains limited to the surrounding structure. Once this overlap length is found, it is sufficient to verify this one configuration with physical tests. In this way, a large share of physical tests can be replaced in future by virtual ones.

However, there is still a lot of work regarding the modelling and simulation requirements from the authorities to do. The purpose of this paper is to provide a practical example of a way in which high-fidelity simulation methods can be used in design and certification in the future.

Funding

This project has received funding from the European Union's Horizon 2020 research and innovation programme under the Grant Agreement No. 807097.

Declaration of competing interest

The authors declare that they have no known competing financial interests or personal relationships that could have appeared to influence the work reported in this paper.

Acknowledgement

We acknowledge support from Master's student Jan Keuntje and Bachelor's student Patrick Makiela for setting up the automated simulation environment.

References

[1] M.J. Turner, R.W. Clough, H.C. Martin, L. Topp, Stiffness and deflection analysis of complex structures, J. Aeronaut. Sci. 23 (9) (1956) 805–823.
[2] M.G. Ostergaard, A.R. Ibbotson, O. Le Roux, A.M. Prior, Virtual testing of aircraft structures, CEAS Aeronaut. J. 1 (1–4) (2011) 83.
[3] C. Lopes, C. González, O. Falcó, F. Naya, J. LLorca, B. Tijs, Multiscale virtual testing: the roadmap to efficient design of composites for damage resistance and tolerance, CEAS Aeronaut. J. 7 (4) (2016) 607–619.
[4] L. Gigliotti, S.T. Pinho, Virtual testing of large composite structures: a multiple length/time-scale framework, J. Multiscale Model. 6 (03) (2015) 1550008.
[5] B. Tijs, C. Lopes, A. Turon, C. Bisagni, J. Waleson, J. van Ingen, S. Veldman, Virtual testing of thermoplastic composites: towards a hybrid simulation-physical testing pyramid, in: ECCM18-18th European Conference On Composite Materials, Athens, Greece, 2018.
[6] Y.A. Gorskii, P. Gavrilov, A. Borovkov, Virtual proving ground for aircraft structures, IOP Conf. Ser. Mater. Sci. Eng. 986 (1) (2020) 012020.
[7] EASA, Modelling & simulation – CS-25 structural certification specifications EASA proposed CM no.: CM-s-014 issue 01, 2020.
[8] C. Soutis, Aerospace engineering requirements in building with composites, in: Polymer Composites In The Aerospace Industry, Elsevier, 2020, pp. 3–22.

[9] J.W. Van Ingen, A. Buitenhuis, M. van Wijngaarden, F. Simmons, Development of the gulfstream G650 induction welded thermoplastic elevators and rudder, in: Proceedings Of The International SAMPE Symposium And Exhibition, Seattle, WA, USA, 2010.
[10] Anonymous, The next generation Multifunctional Fuselage Demonstrator — leveraging thermoplastics for cleaner skies: https://www.cleansky.eu/the-next-generation-multifunctional-fuselage-demonstrator-leveraging-thermoplastics-for-cleaner.
[11] S. Veldman, P. Kortbeek, P. Wölcken, R. Herrmann, J. Kos, I.F. Villegas, Development of a multifunctional fuselage demonstrator, in: Proceedings Of The Aerospace Europe Conference, 2020, pp. 25–28.
[12] P. Liu, J. Zheng, Recent developments on damage modeling and finite element analysis for composite laminates: A review, Mater. Des. 31 (8) (2010) 3825–3834.
[13] Q. Guo, W. Yao, W. Li, N. Gupta, Constitutive models for the structural analysis of composite materials for the finite element analysis: A review of recent practices, Compos. Struct. 260 (2021) 113267.
[14] European Commission, Regulation (EC) No 216/2008 on common rules in the field of civil aviation and establishing a European aviation safety agency, and repealing council directive 91/670/EEC, regulation (EC) No 1592/2002 and directive 2004/36/E, 2008.
[15] European Commission, Commission regulation (EU) No 748/2012 initial airworthiness laying down implementing rules for the airworthiness and environmental certification of aircraft and related products, parts and appliances, as well as for the certification of design and production organisations, 2008.
[16] EASA, AMC 20-29 Composite aircraft structure, 2010.
[17] FAA, AC 20-107B, Composite aircraft structure, 2009, US Department Of Transportation Federal Aviation Administration.
[18] C. Ashforth, L. Ilcewicz, Certification of Bonded Aircraft Structure and Repairs.
[19] S. Waite, Certification and airworthiness of polymer composite aircraft, in: Polymer Composites In The Aerospace Industry, Elsevier, 2020, pp. 593–645.
[20] B. Esp, Practical Analysis Of Aircraft Composites, Grand Oak Publishing, USA, 2017.
[21] F. De Florio, Airworthiness: An Introduction to Aircraft Certification And Operations, Butterworth-Heinemann, 2016.
[22] L. Hart-Smith, The bonded lap-shear coupon–useful for quality assurance but dangerously misleading for design data, 38th int, in: Symp. And Exhib., Anaheim, CA, May, 1993.
[23] I. Ashcroft, M.A. Wahab, A. Crocombe, D. Hughes, S. Shaw, The effect of environment on the fatigue of bonded composite joints. Part 1: testing and fractography, Compos. A Appl. Sci. Manuf. 32 (1) (2001) 45–58.
[24] M. Davis, D. Bond, Certification of adhesive bonds for construction and repair, in: Proceedings Of The 4th Joint DoD/FAA/NASA Conference On Aging Aircraft, 2000, pp. 15–18.
[25] W. De Goeij, M. Van Tooren, A. Beukers, Composite adhesive joints under cyclic loading, Mater. Des. 20 (5) (1999) 213–221.
[26] M.A. Khan, Development of Rules for the Design of Adhesively Bonded Fibre-Reinforced Plastic Composite Joints in Aerospace Applications (Ph.D. thesis), University of Surrey (United Kingdom), 2018.
[27] K. Ranasinghe, K. Guan, A. Gardi, R. Sabatini, Review of advanced low-emission technologies for sustainable aviation, Energy 188 (2019) 115945.
[28] A. Beukers, E. van Hinte, Designing Lightness, NAI010 publishers, Rotterdam, 2020.
[29] S.L. Omairey, S. Sampethai, L. Hans, C. Worrall, S. Lewis, D. Negro, T. Sattar, E. Ferrera, E. Blanco, J. Wighton, et al., Development of innovative automated solutions for the assembly of multifunctional thermoplastic composite fuselage, Int. J. Adv. Manuf. Technol. 117 (5) (2021) 1721–1738.
[30] C. Ageorges, L. Ye, M. Hou, Advances in fusion bonding techniques for joining thermoplastic matrix composites: a review, Compos. A Appl. Sci. Manuf. 32 (6) (2001) 839–857.
[31] A. Yousefpour, M. Hojjati, J.-P. Immarigeon, Fusion bonding/welding of thermoplastic composites, J. Thermoplast. Compos. Mater. 17 (4) (2004) 303–341.
[32] C. Niu, Airframe Stress Analysis And Sizing, AD Adaso/Adastra Engineering LLC, 1997.
[33] A. Skorupa, M. Skorupa, Riveted Lap Joints In Aircraft Fuselage: Design, Analysis And Properties, Vol. 189, Springer Science & Business Media, 2012.
[34] W. Flugge, Stress problems in pressurized cabins, 1952.
[35] Y. Liu, S. Lemanski, X. Zhang, Parametric study of size, curvature and free edge effects on the predicted strength of bonded composite joints, Compos. Struct. 202 (2018) 364–373.
[36] S. Parida, A. Pradhan, Influence of curvature geometry of laminated FRP composite panels on delamination damage in adhesively bonded lap shear joints, Int. J. Adhes. Adhes. 54 (2014) 57–66.
[37] L.F.M. da Silva, R.D.S.G. Campilho, Advances In Numerical Modeling Of Adhesive Joints, Springer Berlin Heidelberg, 2011.
[38] N.J. Al-Ramahi, R. Joffe, J. Varna, Investigation of end and edge effects on results of numerical simulation of single lap adhesive joint with non-linear materials, Int. J. Adhes. Adhes. 87 (2018) 191–204.
[39] O. Völkerink, E. Petersen, J. Koord, C. Hühne, A pragmatic approach for a 3D material model considering elasto-plastic behaviour, damage initiation by puck or cuntze and progressive failure of fibre-reinforced plastics, Comput. Struct. 236 (2020) 106280.
[40] C. Sun, J. Chen, A simple flow rule for characterizing nonlinear behavior of fiber composites, J. Compos. Mater. 23 (10) (1989) 1009–1020.
[41] E. Petersen, R. Cuntze, C. Hühne, Experimental determination of material parameters in cuntzes failure-mode-concept-based UD strength failure conditions, Compos. Sci. Technol. 134 (2016) 12–25.
[42] C. Sun, K. Yoon, Characterization of elastic-plastic behavior of AS4/PEEK thermoplastic composite for temperature variation, J. Compos. Mater. 25 (10) (1991) 1297–1313.
[43] M. Kawai, Y. Masuko, Y. Kawase, R. Negishi, Micromechanical analysis of the off-axis rate-dependent inelastic behavior of unidirectional AS4/PEEK at high temperature, Int. J. Mech. Sci. 43 (9) (2001) 2069–2090.
[44] C. Sun, Y. Rui, Orthotropic elasto-plastic behavior of AS4/PEEK thermoplastic composite in compression, Mech. Mater. 10 (1–2) (1990) 117–125.
[45] D.R. Carlile, D.C. Leach, D.R. Moore, N. Zahlan, Mechanical properties of the carbon fiber/PEEK composite APC-2/AS-4 for structural applications, in: Advances In Thermoplastic Matrix Composite Materials, ASTM International, 1989.
[46] J. Chen, E. Morozov, K. Shankar, A combined elastoplastic damage model for progressive failure analysis of composite materials and structures, Compos. Struct. 94 (12) (2012) 3478–3489.
[47] Z.P. Bažant, B.H. Oh, Crack band theory for fracture of concrete, Matér. Constr. 16 (3) (1983) 155–177.
[48] P.P. Camanho, C.G. Davila, M. De Moura, Numerical simulation of mixed-mode progressive delamination in composite materials, J. Compos. Mater. 37 (16) (2003) 1415–1438.
[49] W. Cui, M. Wisnom, M. Jones, A comparison of failure criteria to predict delamination of unidirectional glass/epoxy specimens waisted through the thickness, Composites 23 (3) (1992) 158–166.
[50] P.P. Camanho, C.G. Dávila, Mixed-mode decohesion finite elements for the simulation of delamination in composite materials, 2002.
[51] A. De Morais, Cohesive zone beam modelling of mixed-mode I–II delamination, Compos. A Appl. Sci. Manuf. 64 (2014) 124–131.
[52] M.L. Benzeggagh, M. Kenane, Measurement of mixed-mode delamination fracture toughness of unidirectional glass/epoxy composites with mixed-mode bending apparatus, Compos. Sci. Technol. 56 (4) (1996) 439–449.
[53] M. Lafarie-Frenot, F. Touchard, Comparative in-plane shear behaviour of long-carbon-fibre composites with thermoset or thermoplastic matrix, Compos. Sci. Technol. 52 (3) (1994) 417–425.
[54] A. Smiley, A. Halbritter, F. Cogswell, P. Meakin, Dual polymer bonding of thermoplastic composite structures, Polym. Eng. Sci. 31 (7) (1991) 526–532.
[55] P. Davies, W. Cantwell, P.-Y. Jar, P.-E. Bourban, V. Zysman, H. Kausch, Joining and repair of a carbon fibre-reinforced thermoplastic, Composites 22 (6) (1991) 425–431.
[56] S. Todd, Joining thermoplastic composites, in: Proceedings Of The22nd International SAMPE Technical Conference, 1990.
[57] A. Beevers, Welding: the way ahead for thermoplastics, Engineering(London)(UK) 231 (10) (1991).